

## **Additive manufacturing fabrication methods and their effects on the fatigue properties of advanced structural alloys**

Jiangjing Xi<sup>1</sup>, Yun Hu<sup>2</sup>, Jun Jiang<sup>3</sup>, Kamran Nikbin<sup>4</sup>

<sup>1</sup> Ph.D. student, Department of Mechanical Engineering, Imperial College London, London, UK  
(j.xi18@imperial.ac.uk)

<sup>2</sup> School of Mechatronics Engineering, Nanchang University, Nanchang 330031, China

<sup>3</sup> Senior Lecturer, Department of Mechanical Engineering, Imperial College London, London, UK

<sup>4</sup> Professor of Structural Integrity, Department of Mechanical Engineering, Imperial College London, London, UK

### **ABSTRACT**

Additive manufacturing is a potential technology which enables the production of metallic components directly from a 3D CAD model with high flexibility and low material waste. The layer-by-layer building method also offers the possibility of manufacturing structure with complex geometry by light weight and force transmission optimization design. The challenge for the AM components is the unclear understanding of the failure behaviors. The low cycle fatigue (LCF) properties of additive manufactured (AM) components (Ti-6Al-4V)(Sterling, Torries, Shamsaei, Thompson, & Seely, 2016) are found to be generally inferior to wrought standard and this restrict its widely application in industry. Optimized fabrication methods and post heat treatment can help enhance the LCF fatigue properties of AM components. In this study, standard cyclic fatigue and monotonic tensile testing specimens were fabricated by AM with different sintering rates, subsequently, heat treated using the standard heat treatment method to release the residual stress. The effects of heat treatment methods and sintering rates on the failure mechanisms of LCF are observed and summarized relating to the data in literature.

### **Introduction**

Additive manufacturing (AM) is a novel process idea which has developed for decades from 1980 s building components using the layer-by-layer method directly from a 3D CAD model(Frazier, 2014). Processes such as Power Bed Fusion (PBF), utilize a laser as energy to melt metal material powder and join the deposited materials layer by layer and process is repeated until the part is generated(Sterling et al., 2016). The PBF methods including Selective Laser Melting also offers the possibility of repairing components and

The manufacturing concept of AM make it capable of fabricating innovative products with complex geometry and realize the aim of light wight design and material efficient. As the mostly widely used titanium alloy, Ti-6Al-4V covers over 50% of the titanium alloy application in the world especially with the aerospace field with more usage than 80% due to its high specific strength, good corrosion resistance, and high strength weight ratio (Donachie, 2000). However, the material and manufacturing cost is expensive for the high requirements of the components. This make the AM technology very potential for building Ti-6Al-4V component especially in the Aerospace fields(Banerjee & Williams, 2013). In general, with the improvement of the AM technology, the tensile properties of AM structures are comparable to the traditional wrought counterparts(Lewandowski & Seifi, 2016). However, the low cycle fatigue (LCF) properties are scattering and inferior to standard manufactured Ti-6Al-4V parts(Amanda Sterlinga, Nima Shamsaeia, b\*, Brian Torriesa, 2015).

Researchers have paid efforts on investigating the LCF properties and the microstructure, internal defects, surface roughness and residual stress are found to have effects on the LCF performance(Åkerfeldt, Pederson, & Antti, 2016). Moreover, the optimized process parameters and post heat treatment methods(Sames, List, Pannala, Dehoff, & Babu, 2016) would improve the fatigue properties.

The aim of this paper is to understand the LCF failure behaviors and fracture mechanism. The standard LCF samples of different manufacturing parameters and heat-treated methods were conducted at four strain level and the experiment results were analyzed and compared to the data collected from literature.

With fracture surface observation and microstructure investigation using SEM and Optical Microscopy, the key factors which influence the LCF properties were summarized and concluded.

### Materials and methods

The samples are additively fabricated in an atmosphere with oxygen less than 10 ppm by an EOS 280 3D printing system. Figure 1 exhibit the SLM samples blocks and final geometry at two sintering rates and heat-treated methods. The Ti-6Al-4V spherical powder with a size between 13 and 65  $\mu\text{m}$  in diameter with the average chemical composition of 6.2 wt.% Al, 3.97 wt.% V and the balance Ti. The samples are built with two different sintering rates (1200  $\text{mm/s}$  and 1300  $\text{mm/s}$ ) but with same standard heat treatment method, and another set of samples were built with 1200  $\text{mm/s}$  and treated by hot isostatic pressing (HIP) method. The left process parameter are as follows: sintering power 280W, layer thickness 40 $\mu\text{m}$ , respectively. Standard heat treatment (800 °C for 4 h) in this study were operated to release the residual stress in the AM parts and HIP treatment (920°C 120MPa for 2 h) is expected to remove the anisotropy and improve the internal defects.



Figure 1. Samples fabrication and post machining. (a) Deposited samples blocks, (b) Final geometry of LCF samples, (c) Final geometry of static tensile samples.

Strain-controlled LCF tests were carried out using a universal testing unit (INSTRON 8802 MTB16002) at room temperature conditions with fully reversed load ratio ( $R_\epsilon = -1$ , triangle waveform) at four strain levels ( $\Delta\epsilon_t/2 = 0.8\%$ , 1.0%, 1.2%, and 2.0% respectively) with extensometer of 12.5mm gauge length. To obtain the reliable LCF results, three samples were conducted at the given strain amplitude. For LCF test the higher strain level will lead to smaller scatter which means it is acceptable for only 1-2 samples to be performed at the highest strain level at 2.0%. Before LCF tests, static tensile tests were conducted at room temperature conditions on the all types of cylindrical samples under the same manufacturing conditions shown in Figure 1(c) using a servo-hydraulic universal testing unit (INSTRON D638, USA) in accordance with the ASTM E8/E8M standard with gauge diameter of 8 mm, gauge length of 25mm. The experiment set up of the static tension and LCF test are shown in Figure 2.

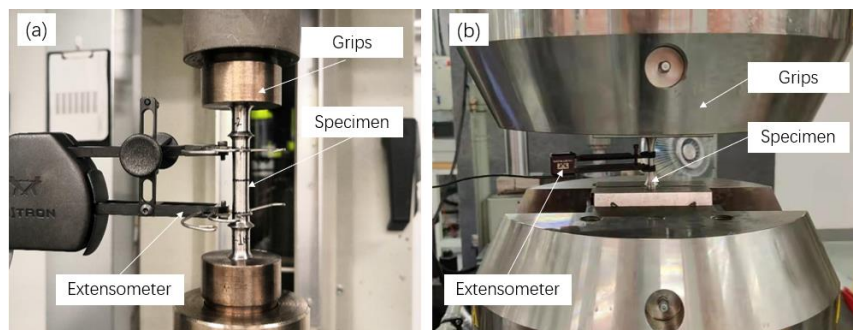


Figure 2. Set up of (a) static tension and (b) LCF test.

The microstructure observation was conducted by using an optical microscope (Zeiss Axio optical). The portions of all the samples which were selected randomly and cut along the longitudinal planes, and processed through standard grinding, polishing and etching (Kroll's reagent, 2% HF, 6% HNO<sub>3</sub>, and 92%

H<sub>2</sub>O). The fracture surface investigation was performed with a Scanning Electron Microscopy (SEM) machine on all types of samples after failure.

The approach to estimate the strain-controlled LCF experiment is described by using Basquin-Coffin-Manson relationship (Muralidharan & Manson, 1988) shown as below in Equation(1)-(4). The total strain was divided into the elastic strain ( $\Delta\varepsilon_e/2$ ) and plastic strain ( $\Delta\varepsilon_p/2$ ) portions. The parameters  $\sigma'_f$  here is the fatigue strength coefficient,  $\varepsilon'_f$  represents the fatigue ductility coefficient, b and c are the fatigue strength exponent and the fatigue ductility exponent respectively.

$$\Delta\varepsilon/2 = \Delta\varepsilon_e/2 + \Delta\varepsilon_p/2 \quad (1)$$

$$\Delta\varepsilon_e/2 = \frac{\sigma'_f}{E} (2N_f)^b \quad (2)$$

$$\Delta\varepsilon_p/2 = \varepsilon'_f (2N_f)^c \quad (3)$$

$$\Delta\varepsilon/2 = \frac{\sigma'_f}{E} (2N_f)^b + \varepsilon'_f (2N_f)^c \quad (4)$$

The cyclic strain-stress properties can be determined by the half-life cycles hysteresis loops in the LCF experiment results. The following equation (Ramberg-Osgood equation)(Suresh, 2012)(ASTM, 2004), in where  $K'$  is the cyclic strength coefficient and  $n'$  is the cyclic strain hardening exponent, to express the cyclic stress-strain relationship by fitting the cyclic stress-strain curves:

$$\frac{\Delta\varepsilon}{2} = \frac{\Delta\sigma}{2E} + \left( \frac{\Delta\sigma}{2K'} \right)^{1/n'} \quad (5)$$

## Results and discussion

Figure 3 presents the initial microstructure features of the three types of samples including the two different building rate and different heat treatment methods. As shown in the Figure 3a and b, the microstructure of the SLM manufactured samples exhibit  $\alpha'$  fine matensite which was formed in the process due to temperature gradient. It can be inferred that slightly higher sintering rate can lead to slight growth of the martensite. The transformation of  $\beta$  and  $\alpha'$  martensite is significantly influenced by the energy input rate and cooling rate(Li, Xu, Zhang, & Kucukkoc, 2018). However, when the material was processed by HIP which is treated with the pressure and temperature lower than the transus temperature for Ti-6Al-4V, it is noticeable that the sub transus temperature process decomposed the martensite  $\alpha'$  into  $\alpha$  and  $\beta$ , lead to the growth of the  $\alpha$  laths, similar results can be found in previous work (Xi et al., 2021). The average size of the grains of the samples selected from the three types of samples were shown in Figure 3d. The results shown here indicate that higher power input thermal process and post heat treatment like HIP treatment can lead to growth of the grain size.

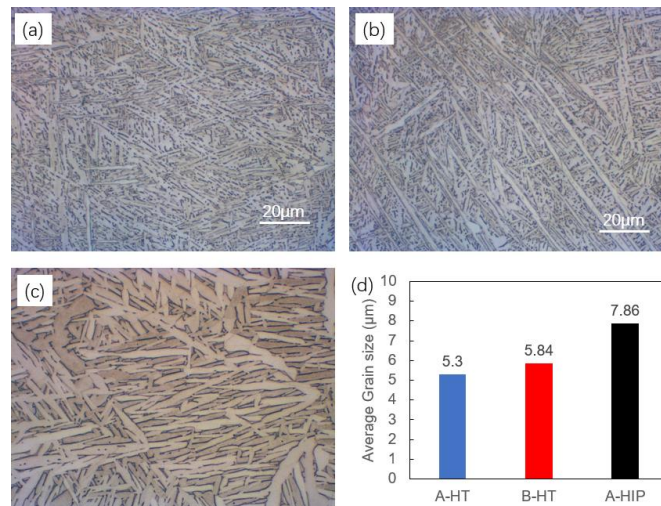


Figure 3. Microstructure of (a) 1200 mm/s built with standard heat treatment (b) 1300 mm/s built with standard heat treatment, (c) 1200 mm/s built with HIP, (d) Average size of the grains.

Figure 4 presents the low cycle fatigue properties and comparison of the SLM manufactured samples at two sintering rates and heat treatment methods. The difference between the same sintering rates of the samples is not easy to distinguish. This is due to the scatter in the experiment data result from the inhomogeneous microstructure features as well as the randomly distribute internal defects (lack of fusion, pores) in the samples. In the previous work(Xi et al., 2021), the Manson-Coffin fitting curve was calculated and analyzed using the half-life stress-strain curve and cyclic elastic modulus. To obtain more accurate data and make comparison of the three batches of data, the parameter used for calculation and analysis is static tensile result from repeating experiment. The modified fitting curves of the 1200 mm/s printed samples (A-HT and A-HIP treated) were shown in Figure 4a,c. Comparing to the 1200 mm/s printed samples the samples manufactured at 1300 mm/s velocity (B-HT) have similar LCF properties at the strain level of 1% but prior to the other two types of samples in the left range of strain amplitude both higher or lower strain amplitude.

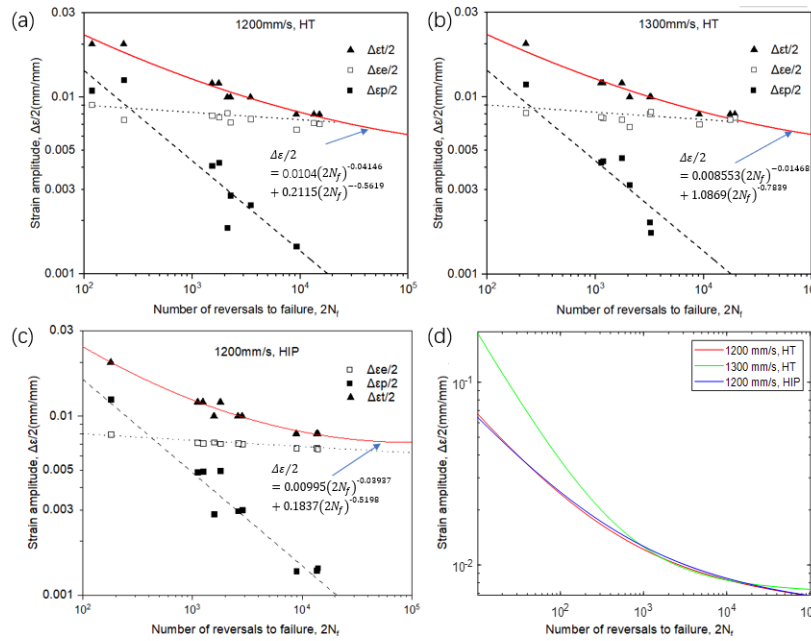


Figure 4. Low cycle properties of the SLM manufactured samples at two sintering velocities and heat treated. (a, b) Strain amplitude range ( $\epsilon_t/2$ )and reversals to failure ( $2N_f$ ) at 1200 mm/s and 1300 mm/s built velocities with standard heat treatment(Xi et al., 2021) (c) Strain amplitude range ( $\epsilon_t/2$ )and reversals to failure ( $2N_f$ ) at 1200 mm/s built with HIPed.

From the static tensile and LCF fatigue test parameters, it can be found that all the three types of samples have similar static tensile performance parameters, which means that the process parameters of the samples are the key factor which decide the tensile properties and the heat treatment method does not play the key role. Comparing to the standard heat-treated samples (A-HT and B-HT), HIPed samples exhibits better ductility but the difference is not obvious. However, the fatigue strength exponent and ductility coefficient are close to each other for the samples manufactured with the same sintering velocity even the heat treatment process is significantly different. The fast-sintering rate led to the scatter of the fatigue lives of the samples as well as the fatigue parameters.

To better understand the LCF properties and mechanisms of the SLM Ti-6Al-4V samples, the detailed fatigue data under the strain amplitudes was investigated. The typical strain-stress curve was picked from all the types of samples and all the samples exhibit cyclic softening phenomena which is the general behavior when subjected to fatigue loading(Suresh, 2002). The strain-stress hysteresis loop at the typical stress level ( $\epsilon_t/2=1.2\%$ ) presents the cyclic softening behavior which was also observed in the other strain amplitudes ( $\epsilon_t/2=0.8\%$ ,  $1.0\%$ ,  $2.0\%$ ). The stress decreased with increase of the loading cycles. In addition, the HIPed samples exhibit a continuing softening behavior until the 90% of cyclic life which demonstrate that the microstructure has effect on the cyclic softening phenomena.

Fracture morphology of the LCF specimens of all process methods at three strain levels (0.8%, 1.0%, 1.2%) were investigated. The fatigue fracture surface including initiation location and crack growth region of the samples are shown in Figure 5. All cracks initiated at subsurface or near surface region which is a flat area, as shown in the white dot circle in Figure 5. The fracture surface of samples at various strain amplitudes shows different features which means that the strain level can affect the fracture morphology significantly for all these samples. In addition, the internal defects which is expected to be the crack initiation location were not observed in the crack initiation region. There are voids and lack of fusion defects found in the fracture surface but not in the subsurface area or crack initiation point which demonstrate internal defects are not the key contribution to LCF properties.

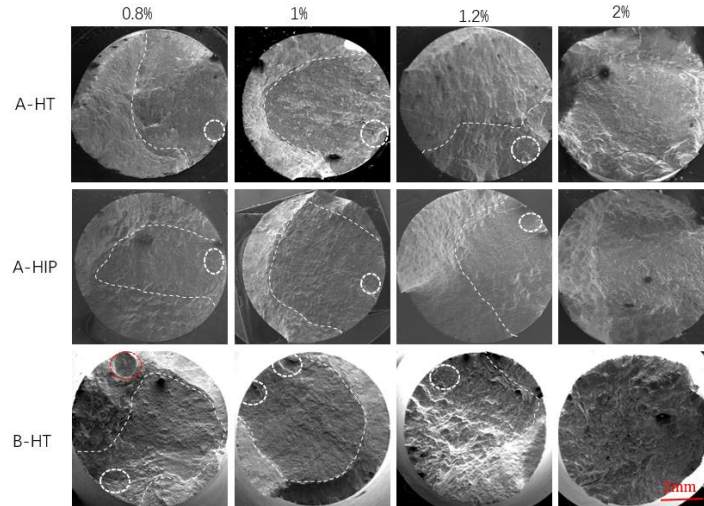


Figure 5. Low cycle fatigue fractography of all the SLM manufactured samples at all the strain amplitudes.

To further evaluate the roles of the internal defects on the LCF performance, investigation focusing on the internal defects were conducted by SEM and the typical defects are shown in the Figure 6. It is noted that no defects were found in the fracture surface of the HIPed samples. This indicate that the HIP process can help improve the internal defects significantly. Both the samples with standard heat treated at 1200 mm/s and 1300 mm/s printed velocity contain defects. In addition, more defects located in the fracture surface of the 1300 mm/s sintered samples. The equivalent diameter of defect size of the slow printed samples is around 15-25  $\mu\text{m}$  and the value of 1300 mm/s printed samples is 20-80  $\mu\text{m}$ . These findings indicate that higher sintering rate can introduce more voids in the manufacturing process.

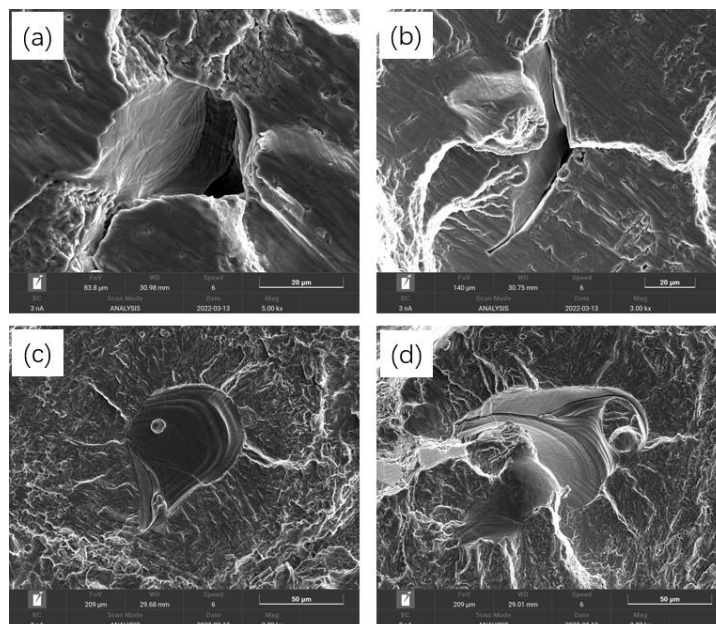


Figure 6. Typical internal defects observed in the fracture surface.

The fatigue performance of Ti-6Al-4V materials manufactured by AM technology depends on the material manufacturing quality including microstructure and internal defects. Therefore, we compared the LCF experiment results data of many types samples manufacture with many kinds of process parameters from publications(Ren et al., 2019)(Benedetti, Fontanari, Bandini, Zanini, & Carmignato, 2018)(“Aeronautical China. Materials Handbook, Vol 4: Titanium alloys and Copper Alloys 2001:104–32.” n.d.)(Amanda Sterlinga, Nima Shamsaiea, b\*, Brian Torriesa, 2015) to investigate the relationship between the manufacturing parameters and LCF properties. Normally there is great scatter in the low cycle fatigue life for the Ti-6Al-4V at given strain level. To eliminate the fatigue data scatter, Coffin-Manson equation is used to unify the data and make the comparison of all the results. The difference between the curves demonstrates the wrought samples has the most balanced properties both at high and low strain amplitudes. The SLM with 1200 mm/s or 1300 mm/s building velocity samples have better LCF properties than other AM Ti-6Al-4V samples.

According to the data, we found that yield stress and ductility of AM parts play an important role in deciding the LCF properties. The as-built Ti-6Al-4V has higher yield stress value but poor ductility. When the samples were manufactured using similar process parameters, samples have similar LCF properties but higher ductility will lead to better LCF life at lower strain levels. Furthermore, another factor on the LCF lives is the micro structure feature like the  $\alpha$ -phase and prior- $\beta$  grains size(Ren et al., 2019). In this work, it is noted that the 1300 mm/s printed samples with standard heat treatment have the prior ductility than the other two types, and when it comes to the high strain level, the fast built samples contain coarser grains than samples with same heat treatment method but slower built which led to the higher resistance at high strain levels. Therefore, improvement of yield stress can lead to the increase of LCF at high strain amplitudes, while the increase of tension elongation makes the enhancement of LCF life at low strain levels. It can be inferred that the wrought materials have the balanced properties at both low and high strain amplitudes. With the increase of both the yield stress and ductility, the LCF properties can be improved at all strain amplitudes.

Further comparison of the LCF life  $N_f$  of the tree types of samples at all strains amplitudes are shown in Figure 7. The relationship between the max stress response of each sample and the cycles to failure were also summarized and presented in Figure 8. It can be indicated from the following two figures that the 1300 mm/s printed samples exhibit noticeable dispersity in both the cyclic life and the stress response in the loading process. And this demonstrates the power input and thermal process has a critical effect on the material properties and stress behaviors. The similar behavior can be observed in the A-HT samples. In addition, the higher sintering velocity can slightly enhance the LCF life though the dispersity increases. The post treatment also plays critical role on improvement the fatigue properties especially the concentration degree of the LCF results data. This behavior can also be verified in the stress response performance. This means that HIP treatment process can help to improve the material properties and decrease the data dispersity of the fatigue performance. In addition, it can be inferred that the corresponding relationship of stress response and fatigue life exist.

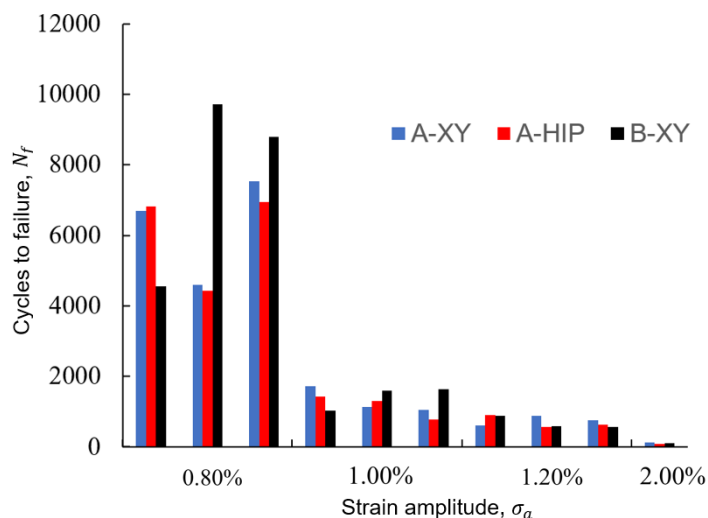


Figure 7 Number of cycles to failure for LCF of the samples.

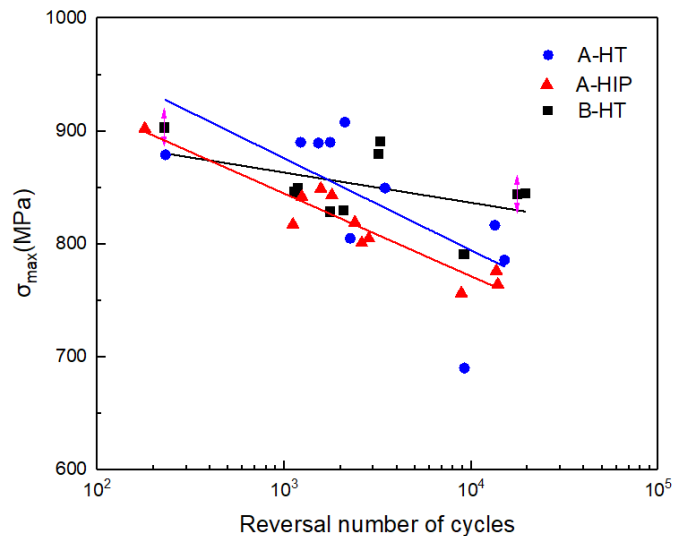


Figure 8 Number of cycles to failure for LCF of the samples.

## Conclusions

The major conclusions can be summarized as follows. (i) Tensile properties of 1200 mm/s printed HT and HIPed and 1300 mm/s printed SLM Ti-6Al-4V alloy are similar and comparable to the wrought counterparts. (ii) The three types of SLM Ti-6Al-4V alloy exhibit higher LCF lives than those AM Ti-6Al-4V in the references. (iii) With the increase of the strain amplitudes, the cyclic softening degree increased. (iv) HIP process helps to close the internal defects and almost no defects are found in HIPed samples. Defects were found in the HT samples fracture surface which can be inferred that the defects are not the dominant factor influencing the LCF properties of SLM Ti-6Al-4V, furthermore, the interior defects are not detrimental to LCF performance. (v) Both yield stress and elongation of AM Ti-6Al-4V parts increase, and the LCF life will be improved at all strain levels. (vi) HIP treatment can help to improve the fatigue property and results concentration degree.

## Acknowledgement

The strong support from the Aviation Industry Corporation of China (AVIC) Aircraft Strength Research Institute (ASRI) for this funded research is much appreciated. The project is also supported by the National Natural Science of China [Grant number. 52165017].

## References

- Aeronautical China. Materials Handbook, Vol 4: Titanium alloys and Copper Alloys 2001:104–32. (n.d.).
- Åkerfeldt, P., Pederson, R., & Antti, M. L. (2016). A fractographic study exploring the relationship between the low cycle fatigue and metallurgical properties of laser metal wire deposited Ti-6Al-4V. *International Journal of Fatigue*, 87, 245–256. <https://doi.org/10.1016/j.ijfatigue.2016.02.011>
- Amanda Sterlina, Nima Shamsaiea, b\*, Brian Torriosa, S. M. T. (2015). Fatigue Behaviour of Additively Manufactured Ti-6Al-4V.
- ASTM. (2004). Standard Test Method for Strain-Controlled Fatigue Testing. *E606/E606M-12*, 96(2004), 1–16. <https://doi.org/10.1520/E0606-04E01>. Copyright
- Banerjee, D., & Williams, J. C. (2013). Perspectives on titanium science and technology. *Acta Materialia*. <https://doi.org/10.1016/j.actamat.2012.10.043>
- Benedetti, M., Fontanari, V., Bandini, M., Zanini, F., & Carmignato, S. (2018). Low- and high-cycle fatigue resistance of Ti-6Al-4V ELI additively manufactured via selective laser melting: Mean stress and defect sensitivity. *International Journal of Fatigue*, 107(October 2017), 96–109. <https://doi.org/10.1016/j.ijfatigue.2017.10.021>
- Donachie, M. J. (2000). *Titanium - A Technical Guide*. ASM International (Vol. 99). Retrieved from <http://www.intechopen.com/books/corrosion-resistance>
- Frazier, W. E. (2014). Metal additive manufacturing: A review. *Journal of Materials Engineering and Performance*, 23(6), 1917–1928. <https://doi.org/10.1007/s11665-014-0958-z>

- Lewandowski, J. J., & Seifi, M. (2016). Metal Additive Manufacturing: A Review of Mechanical Properties. *Annual Review of Materials Research*, 46(1), 151–186. <https://doi.org/10.1146/annurev-matsci-070115-032024>
- Li, Z., Xu, R., Zhang, Z., & Kucukkoc, I. (2018). The influence of scan length on fabricating thin-walled components in selective laser melting. *International Journal of Machine Tools and Manufacture*. <https://doi.org/10.1016/j.ijmactools.2017.11.012>
- Muralidharan, U., & Manson, S. S. (1988). A modified universal slopes equation for estimation of fatigue characteristics of metals. *Journal of Engineering Materials and Technology, Transactions of the ASME*, 110(1), 55–58. <https://doi.org/10.1115/1.3226010>
- Ren, Y. M., Lin, X., Guo, P. F., Yang, H. O., Tan, H., Chen, J., ... Zhang, Y. Y. (2019). Low cycle fatigue properties of Ti-6Al-4V alloy fabricated by high-power laser directed energy deposition : Experimental and prediction, 127(March), 58–73. <https://doi.org/10.1016/j.ijfatigue.2019.05.035>
- Sames, W. J., List, F. A., Pannala, S., Dehoff, R. R., & Babu, S. S. (2016). The metallurgy and processing science of metal additive manufacturing. *International Materials Reviews*, 61(5), 315–360. <https://doi.org/10.1080/09506608.2015.1116649>
- Sterling, A. J., Torries, B., Shamsaei, N., Thompson, S. M., & Seely, D. W. (2016). Fatigue behavior and failure mechanisms of direct laser deposited Ti-6Al-4V. *Materials Science and Engineering A*, 655, 100–112. <https://doi.org/10.1016/j.msea.2015.12.026>
- Suresh, S. (2002). *Fatigue of Materials*. CAMBRIDGE UNIVERSITY PRESS. <https://doi.org/10.1201/9780203910399.ch14>
- Suresh, S. (2012). *Cyclic deformation in ductile single crystals*. *Fatigue of Materials*. <https://doi.org/10.1017/cbo9780511806575.004>
- Xi, J., Hu, Y., Xing, H., Han, Y., Zhang, H., Jiang, J., & Nikbin, K. (2021). The low-cycle fatigue behavior, failure mechanism and prediction of SLM Ti-6Al-4V alloy with different heat treatment methods. *Materials*. <https://doi.org/10.3390/ma14216276>